HHS Public Access

Author manuscript

J Control Release. Author manuscript; available in PMC 2021 May 10.

Published in final edited form as:

J Control Release. 2020 May 10; 321: 363–371. doi:10.1016/j.jconrel.2020.02.021.

Glutathione-responsive biodegradable polyurethane nanoparticles for lung cancer treatment

Roshni Iyer[1], **Tam Nguyen**[1], **Dona Padanilam**[1], **Cancan Xu**[1], **Debabrata Saha**[3], **Kytai T. Nguyen**[1,2,*], **Yi Hong**[1,2,*]

[1]Department of Bioengineering, University of Texas at Arlington, Arlington, TX 76019, USA

[2]Joint Biomedical Engineering Program, University of Texas Southwestern Medical Center, Dallas, TX 75390, USA

[3]Department of Radiation Oncology, University of Texas Southwestern Medical Center, Dallas, TX 75390, USA

Abstract

Lung cancer is one of the major causes of cancer-related deaths worldwide. Stimuli-responsive polymers and nanoparticles, which respond to exogenous or endogenous stimuli in the tumor microenvironment, have been widely investigated for spatiotemporal chemotherapeutic drug release applications for cancer chemotherapy. We developed glutathione (GSH)-responsive polyurethane nanoparticles (GPUs) using a GSH-cleavable disulfide bond containing polyurethane that responds to elevated levels of GSH within lung cancer cells. The polyurethane nanoparticles were fabricated using a single emulsion and mixed organic solvent method. Cisplatin-loaded GSH-sensitive nanoparticles (CGPU) displayed a GSH-dose dependent release of cisplatin. In addition, a significant reduction in *in vitro* survival fraction of A549 lung cancer cells was observed compared to free cisplatin of equivalent concentration (survival fraction of ~0.5 and ~0.7, respectively). The *in vivo* biodistribution studies showed localization of fluorescently labeled GPUs (~7% of total injected dose) in the lung tumor regions after mouse-tail IV injections in xenograft A549 lung tumor models. The animals exposed to CGPUs also exhibited the inhibition of lung tumor growth compared to animals administered with saline (tumor growth rate of 1.5 vs. 13 in saline) and free cisplatin (tumor growth rate of 5.9) in mouse xenograft A549 lung tumor models within 14 days. These nanoparticles have potential to be used for on-demand drug release for an enhanced chemotherapy to effectively treat lung cancer.

Keywords

Glutathione; nanoparticles; lung cancer; cisplatin; stimuli responsive

*Corresponding authors: Yi Hong, yihong@uta.edu, TEL: +1-817-272-0562; FAX: +1-817-272-2251; Kytai T. Nguyen, knguyen@uta.edu, TEL: +1-817-272-2540; FAX: +1-817-272-2251.

1. INTRODUCTION

Lung cancer is one of the most common causes of cancer-related mortality in the United States, with over 230,000 new cancer cases and over 150,000 deaths in the year 2018 [1]. The major variant of lung cancer is non-small cell lung cancer (NSCLC) that accounts for over 85% of these cases, thus there is an urgent need to effectively treat this deadly disease [2]. The anti-neoplastic drug cisplatin (*cis*-diamminedichloroplatinum (II)) has been widely investigated in the clinic to treat various solid tumors, such as head and neck squamous carcinoma and ovarian cancer, and it is the first-line FDA approved treatment for NSCLC [3]. Cisplatin has decreased the overall lung cancer associated mortality by 6.9% compared to that of untreated controls [4]. Although cisplatin has been used in chemotherapy to effectively kill lung cancer cells and reduce lung tumor growth, it has several drawbacks, including severe toxicity in visceral organs and fast clearance resulted in inadequate intra-tumor drug concentrations [5]. Additionally, cisplatin is poorly soluble in aqueous solvents affecting its bioavailability and therapeutic index [6]. The efficacy of cisplatin therapeutics is also limited by innate and acquired drug resistance [3].

The limitations of chemotherapy drugs such as their systemic toxicity, poor plasma-solubility and low bioavailability, can be potentially overcome by encapsulating them into nanoparticles (NPs). NPs as drug carriers for chemotherapy have achieved tremendous popularity because of their small size, and customizability to improve their accumulation in the tumor tissues, thereby improving drug bioavailability and distribution in the tumors [7]. Stimuli-responsive nanoparticles are a class of nanoparticles that observe low drug release in normal physiological conditions and enhance drug delivery at the targeted site upon exposure to a stimulus rendering the ability of spatial, temporal and dose-controlled drug release [8]. Thus, stimuli-responsive nanoparticles are gaining significant insight for treating various cancers that dispense various endogenous stimuli to trigger the drug release from these nanoparticles, such as changes in pH and enzyme levels in the tumor microenvironment [9]. The cancer microenvironment also hosts enhanced levels of molecular species, namely antioxidants like glutathione (GSH), that are upregulated in response to high levels of oxidative stress within the cancer tissues [10]. The GSH levels in the intracellular environment of cancer cells are over 100–1,000 times higher than that in the environment surrounding the cancer cells [8]. This observation has led to the development of redox-responsive polymers comprised of disulfide bonds in the backbone that undergo reduction-mediated cleavage in response to increased levels of GSH, thereby quickly releasing their payloads [8, 9].

Recently, increasing use of GSH responsive nanoparticles for cancer therapy has been witnessed, however, such nanoparticles for lung cancer therapy have been scarcely reported. In this *proof-of-concept* work, we developed a GSH-responsive nanoparticle loaded with an anti-cancer drug and investigated its potential to specifically treat NSCLC in a subcutaneous cancer model. A biodegradable polyurethane comprised of disulfide linkages in the backbone named as PU-SS, has been previously developed in our lab [11]. It exhibited a high degradation rate when exposed to GSH and consisted of good *in vitro* cytocompatibility and *in vivo* tissue compatibility. In our research, the anticancer drug cisplatin was used as a model drug to be encapsulated in PU-SS NPs (Figure 1). The drug release kinetics of

cisplatin from these NPs in response to GSH concentrations was investigated. Their cell compatibility, blood compatibility, cancer cell killing, and cell uptake were assessed *in vitro*. The *in vivo* distribution and therapeutic efficacy of these NPs were further evaluated in a murine subcutaneous lung tumor model using A549 cells (Figure 1).

2. EXPERIMENTAL SECTION

2.1 Materials

Polycaprolactone diol, 1,6-hexamethylene diisocyanate, dimethyl sulfoxide (DMSO), dichloromethane (DCM), hexafluoroisopropanol (HFIP), polyvinyl alcohol (PVA), o-phenylenediamine (OPDA) were purchased from Millipore Sigma. Cisplatin was purchased from Cayman Chemicals. Poly(lactide-co-glycolide) (PLGA 50:50, lactic acid: glycolic acid ratio of 50:50) was purchased from PolySciTech® (Molecular weight of 55–65 KDa). A549 lung cancer cells were purchased from ATCC, and Type I lung epithelial cells (AT1) were purchased from Abmgood.

2.2 Fabrication of PU-SS nanoparticles

Glutathione-sensitive PU-SS polymer was synthesized using polycaprolactone diol (MW=2000) and 1,6-hexamethylene diisocyanate, with hydroxyethyl disulfide (Sigma) in a molar ratio of 0.2:2:1.8 according to Xu et al [11]. Cisplatin loaded PU-SS NPs (CGPU) were prepared by a standard emulsion technique. Briefly, a 10% solution of cisplatin in 200 μl of DMSO was added to a 2% solution of PU-SS dissolved in a solvent mixture of 95% DCM and 5% HFIP. PU-SS is hard to be dissolved in DCM at room temperature, and it is easy to be soluble in HFIP. The HFIP addition helped PU-SS soluble in DCM at room temperature. This solution was then sonicated using a microtip sonicator at 10 watts for 5 minutes, and then added dropwise to 4 ml of 5% PVA, followed by sonication using an ultrasonicator at 30 watts for 5 minutes. Following overnight stirring, NPs were washed with deionized water and collected by centrifugation and lyophilization. Blank PU-SS NPs (GPU), cyanine-7-, or coumarin-6 loaded GPUs (1% w/w of dye to polymer) were also synthesized using the same method described as above. Cisplatin-loaded PLGA 50:50 NPs (CPLGA) were synthesized as described earlier [12]. Briefly, 10% w/w cisplatin/DMSO solution was added to a solution of 3% v/v PLGA 50:50 in DCM and sonicated using a microtip sonicator at 20 watts for 1 minute to mix the solutions. The resulting solution was further added dropwise to a 5% w/v PVA solution (12 ml) and ultrasonicated at 30 watts for 10 minutes while on ice. After overnight stirring and complete solvent evaporation, the NPs were washed and collected via ultracentrifugation and lyophilization.

2.3 Characterization of nanoparticles

Particle size, size distribution, and surface charges were measured using the dynamic light scattering (DLS) technique using a ZetaPALS zeta potential analyzer (Brookhaven Instruments Inc.). Transmission electron microscopy (TEM, JOEL 1200EX) and scanning electron microscopy (SEM, Hitachi S-4800 II FE SEM) were also used to visualize the morphology of these NPs.

For cisplatin loading efficiency, cisplatin in the supernatant collected from the NP fabrication was quantified through an o-phenylenediamine (OPDA) based spectrophotometric detection technique [13]. A mixture of the cisplatin solution (250 μL), 1 ml of 1X PBS (pH 6.8) and 1 ml of OPDA solution (18 mg/ml in 1X PBS, pH 6.8) was heated at 100°C for 10 minutes and cooled down to room temperature, and then 7 ml of dimethylformamide was added. The change in color as a result of the interaction between OPDA and cisplatin was detected by a UV-Vis spectrophotometer at 703 nm (Infinite M200, Tecan Group Ltd). The cisplatin loading efficiency was calculated as:

$$\text{Cisplatin loading efficiency}\ (\%) = \frac{C1 - C2}{C1} \times 100 \quad (1)$$

Where C1 is the amount of cisplatin used in the nanoparticle formulation, and C2 is the amount of cisplatin in the supernatant.

To study the GSH triggered cisplatin release kinetics from the CGPUs, the lyophilized NPs were re-suspended in 0, 5, or 10 mM of GSH (Cayman chemicals) in 1X PBS (pH 7.4) in a 1 mg/ml concentration. The NP suspension (1 ml) was added to a microcentrifuge tube (4 replicates were used for each glutathione concentration) and incubated at 37 °C. At pre-determined time points, the NP suspensions were centrifuged, 1 ml of the supernatants from each tube were collected, and the pellets were resuspended in 1 ml of the same GSH solutions and incubated at 37°C until the next time point. The amount of cisplatin released from the NPs was quantified by the OPDA chemistry as described above. A standard curve of known cisplatin concentrations was used to determine the cumulative cisplatin release. Stability of the NPs was determined by measuring the NP size using DLS when incubated these NPs in 10% FBS, 0.9% saline, or Gamble's solution (simulated human lung fluid) at 37°C for 3 days. A sample size of n=3 per group was used.

2.4 Cytotoxicity analysis of nanoparticles

Lung alveolar Type 1 epithelial cells (AT1) cells were seeded at a density of 8,000 cells/well in a 96 micro-well plate and incubated overnight to facilitate cell attachment. The cells were then incubated with varying concentrations of non-drug loaded GPUs (0, 10, 50, 100, 200, 500, 750 and 1000 μg/ml). After 24 hours incubation, cell viability was determined using MTS cell viability assays (CellTiter 96®AQueous One Solution Cell Proliferation Assay, Promega) and visualized using a live-dead assay (LIVE/DEAD ® Viability/Cytotoxicity Kit for mammalian cells, Invitrogen) according to the manufacturer's instructions.

2.5 Hemocompatibility analysis of nanoparticles

A hemolysis evaluation of the non-drug loaded GPUs was conducted as described previously [14]. Human blood from a donor was acquired in acid citrate dextrose (ACD) containing tubes following methods approved by the Institutional Review Board at the University of Texas at Arlington. After collection, the human blood was incubated with the GPUs at concentrations of 100 μg/ml or 1,000 μg/ml in PBS, 0.9% saline (as negative control), or distilled water (positive control) for 2 hours at 37°C. The samples were then centrifuged at 1,000 g, and their absorbance intensity at 545 nm were recorded using a UV-Vis spectrophotometer. The percentage of hemolysis was calculated using the equation below:

$$\% \text{ Hemolysis} = \frac{A1 - A2}{A3 - A2} \times 100\% \quad (2)$$

Where: A1 = Absorbance of sample at 545 nm; A2 = Absorbance of negative control at 545 nm; and A3 = Absorbance of positive control at 545 nm.

For the blood clotting kinetics, the non-drug loaded GPUs at concentrations of 100 or 1,000 μg/ml), water (negative control), and 0.9% saline (positive control) were added to the human blood activated with 0.1M $CaCl_2$, in 1.5 ml microcentrifuge tubes, and then the tubes were incubated at room temperature. At pre-determined time points (10, 20, 30, and 60 minutes), water was added to the tubes to lyse the red blood cells (RBCs) that were not a part of the formed clot. Absorbance readings of supernatant were recorded at 540 nm using a UV-Vis spectrophotometer. The absorbance intensities are inversely proportional to the size of the resulting clot. A sample size of n=8 per group was used for the hemolysis and blood clotting studies.

2.6 Cellular uptake of nanoparticles

Cellular uptake of GPUs was determined by measuring the amounts of fluorescently labeled NPs internalized by lung cancer cells. Coumarin-6 loaded GPUs were used to facilitate fluorescent mediated detection of the NPs in the cells. A549 human lung cancer cells were seeded at a seeding density of 10,000 cells/well in a 96 micro-well plate. After overnight attachment, the cells were incubated with GPUs at different concentrations (0, 50, 100, and 250 μg/ml) at 37°C for 2 hours. After 2 hours, the cells were washed 3X with sterile 1X PBS, and then lysed using 1% Triton X-100. The amount of internalized NPs was determined by measuring the fluorescence intensity of coumarin-6 (translated to μg of NPs) at a wavelength of λex 458 nm and λem 540 nm and normalized against the amount of total protein from cells per well, determined using bicinchonic acid assay (BCA) as per the manufacturer's protocol (Pierce™ BCA Protein Assay Kit, Thermo Scientific).

The cellular uptake of GPUs by A549 lung cancer cells was also visualized by fluorescence imaging. A549 cells were seeded at a cell seeding density of 15,000 cells/chamber on an 8-chamber slide and allowed to attach overnight. Then, the A549 cells were exposed to 50 μg/ml, 100 μg/ml, and 250 μg/ml of coumarin-6 loaded GPUs for 2 hours, following 3X rinse with PBS, and then the cells were fixed for 30 minutes in 4% paraformaldehyde. The fixed cells were then washed with PBS to remove excess paraformaldehyde, and their nucleus stained with NucBlue (Thermoscientific). The cells were then observed under a fluorescence microscope (Cytoviva, Inc.).

2.7 *In vitro* lung cancer cell killing studies

The *in vitro* cancer killing efficacy of CGPUs was determined by lactate dehydrogenase (LDH) cytotoxicity assays. Briefly, A549 lung cancer cells were seeded at a seeding density of 20,000 cells/well in a 48 micro-well plate and cultured overnight. The cells were then treated with 1 mL per well of free cisplatin (3 μg/ml or 5 μg/ml drug concentration) or NPs: CGPUs, and cisplatin loaded PLGA NPs (CPLGA) (NP concentration equivalent to 3 μg/ml and 5 μg/ml of cisplatin determined from the drug release kinetics) for 72 hours. In case of

bare GPUs (no drug), the cells were treated with equivalent amounts of NPs as that of the CGPUs (corresponding to 60 μg/mL and 100 μg/mL for the 3 μg/mL and 5 μg/mL cisplatin groups, respectively). Untreated cells and cells treated with 1% Triton were used as the negative and positive controls, respectively. After 72 hours, cell death was determined by LDH cytotoxicity assays per the manufacturer's instruction. *In vitro* cancer cell death was further verified using live/dead cell staining (Enzo Lifesciences) following the manufacturer's protocol.

In vitro cancer cell killing efficacy was also confirmed by quantifying the caspase-3 expression, as a marker for cell apoptosis after treatment. The A549 lung cancer cells were seeded at an initial seeding density of 250,000 cells/flask in T-25 flasks. Once the cells reached confluency, they were treated with free cisplatin (5 μg/ml) or NPs: CGPUs, CPLGA (concentration equivalent to 5 μg/ml of cisplatin determined from the drug release kinetics) for 72 hours. Similar to the previous study, the concentration of GPUs exposed to the cells was equivalent to that of CGPUs used. Untreated cells and cells exposed to 10% DMSO for the same period as the treatment groups served as the negative and positive control, respectively. After 72 hours, caspase-3 expression in the cells was detected by EnzChek™ caspase-3 assay kit #1 (Thermofisher Scientific) following the manufacturer's protocol.

To observe the survival of cancer cells upon exposure to the CGPU NPs, colony formation assays were performed. Colony formation assay (CFA) is used to establish the ability of individual cells to survive and undergo cellular division, forming their individual colonies [15]. The effects of therapeutic reagents are reflected in the ability of the cancer cells to form their colonies after exposure to these agents. Colonies comprising of more than 50 cells are considered as one colony and counted. The A549 lung cancer cells were seeded on 60 mm petri-dishes, and *in vitro* CFA studies were performed as described previously [16]. The cells were treated with free cisplatin (100 ng/dish) or NPs such as CGPUs and CPLGA (concentration equivalent to 100 ng/dish of cisplatin) and incubated at 37°C for 10 days. A549 lung cancer cells without treatment were included as controls. Blank NPs or GPUs were also studied for comparison. When the cancer cell colonies had reached a colony of at least 50 cells, the cells were rinsed with phosphate buffered saline and stained with crystal violet dye (0.5% w/v in 6% v/v glutaraldehyde). The number of colonies in each dish was then counted. A sample size of n=3 per group was used.

2.8 *In vivo* biodistribution of fluorescently labeled nanoparticles

To detect the *in vivo* biodistribution of GPUs, athymic nude mice (Foxn1^{nu}, Jackson labs) were implanted with A549 lung cancer cells (2 million cells) subcutaneously in the hind-limb, following the protocol approved by the Institutional Animal Care and Use Committee (IACUC) at the University of Texas at Arlington. When the tumors reached a diameter of approximately 10 mm, treatment was commenced. 0.9% saline served as a negative control, while cyanine-7 loaded GPUs served as the study groups. Animals were injected with saline or 1.5 mg of the NPs (n=4 per group) intravenously. 24 hours post NP administration, the mice were euthanized, and their tumors and visceral organs excised for fluorescence imaging using an *in vivo* bioimager (Kodak In vivo Fx Pro system). The tissues were further homogenized using a tissue homogenizer (Precellys evolution, Bertin Instruments), followed

by centrifugation and the supernatant read using a UV-*Vis* spectrophotometer (Infinite M200, Tecan Group Ltd) at wavelengths of Excitation: 760nm and Emission: 830nm. The concentration of GPUs in the tissue was calculated using a standard curve of cyanine 7 loaded GPUs and reading the sample value in a spectrophotometer at wavelengths of Excitation: 760nm and Emission: 830nm. To estimate the amount of GPUs accumulated in the tissues, we then calculated the percentage of injected dose (ID) per gram tissue (% ID/g) using Equation 3 below [17].

$$\%\ \text{NP localization in tissue} = \left(\frac{\text{Amount of NPs in tissue specimen}}{\text{Total amount of NPs administered}} \times 100\right) / \text{weight of tissue in gram} \quad (3)$$

2.9 *In vivo* lung tumor therapeutic efficacy study

For the *in vivo* therapeutic efficacy of the CGPUs, athymic nude mice (Foxn1^{nu}, Jackson labs) were implanted with A549 lung cancer cells as described earlier. The treatment was executed when the tumors reached a diameter of 7 mm measured by a caliper. The saline (0.9%) served as a negative control. The study groups included free cisplatin (2.5 mg/kg per dose) and NPs, including GPUs and CGPUs (at an equivalent dose of 2.5 mg/kg cisplatin per dose). Six randomly allocated mice per group (3 males and 3 females) were used. The animals were injected with the control or study group dose via tail vein injection twice per week. Body weight (g) and tumor diameters (mm) were measured before each dosing regimen. Once the tumors in the control saline group reached a diameter of 20 mm, the study was considered to reach the endpoint. Then the animals were euthanized, and their tumors excised and fixed in 4% paraformaldehyde (4% PFA). The lungs, heart, kidneys, liver, and spleen were also collected and fixed in 4% PFA. The tumor volumes were determined by the following:

$$\text{Tumor volume} = \left(\left(\text{tumor width}^2\right) \times \text{tumor length}\right)/2 \quad (4)$$

Tumor growth rates (TGR: V/V_0) were calculated by normalizing tumor volumes (V) at a specific time to the tumor volume at the start of NP/drug administration (V_0) using equation:

$$\text{Tumor growth rate} = V/V_0 \quad (5)$$

2.10 Statistical analysis

Results were analyzed statistically using 2-way ANOVA and Fisher's post-hoc analysis (Statview 5.0 software) with $p<0.05$ considered as a significant value. All results are displayed as mean ± SD, and quadruplet samples were used for each experiment if not specified.

3. RESULTS

3.1 Nanoparticle characteristics

The biodegradable polyurethane nanoparticles were fabricated using a single emulsion technique and mixed organic solvent method. The GPUs and CGPUs had a mean diameter of 189±21 nm and 245±20 nm, respectively (Figure 2A). The zeta potentials of GPUs and CGPUs were determined to be −14±4 mV and −12±2 mV, respectively (Figure 2A). TEM and SEM images revealed a spherical, smooth morphology of the CGPU NPs (Figure 2B).

The stability of the GPUs in 0.9% saline, complete media (supplemented with 10% FBS), and gamble's solution was determined by measuring the NP size at various time points using dynamic light scattering (Figure 2C). Stable NP sizes up to 48 hours were observed in all three solutions. The drug loading efficiency of cisplatin in the CGPUs was measured (Equation 1) to be about 55%. Cisplatin release kinetics observed a GSH dose dependent increase in the amounts of drug release. Nanoparticles exposed to 5 mM and 10 mM of GSH released nearly 5 times and 8 times higher drug release respectively compared to 0 mM of GSH, within 100 hours of exposure time (Figure 2D). A higher drug release at elevated GSH concentrations could potentially result from faster and greater breaking of the disulfide links in the nanoparticle backbone, thereby accelerating drug release from the nanoparticles. The enhanced drug release upon exposure to elevated GSH levels thus confirms the GSH responsiveness of the nanoparticle formulation.

3.2 *In vitro* cytocompatibility, hemocompatibility, and cell uptake

The cytocompatibility of GPUs at increasing concentrations was determined by MTS assays (Figure 3A) and live/dead staining (Figure 3B). The GPUs exhibited over 90% cyto-compatibility up to 500 μg/ml, and more than 80% cell viability at the highest NP concentration of 1000 μg/ml to AT1, showing a good cyto-compatibility of the NPs to the healthy lung cells.

The hemocompatibility of the GPUs were evaluated through the hemolysis of blood and blood clotting profile of the human whole blood exposed to the GPUs. The GPUs showed less than 1% hemolysis, which is much lower than the acceptable range for hemolysis. Furthermore, the effects of GPUs on the blood clotting kinetics were evaluated by comparing to the blood exposed to 0.9% saline (positive control) over 60 minutes. The general clotting trend for blood treated with GPUs was observed to follow that of blood treated with 0.9% saline, where blood progressively clotted within 20 minutes of exposure to the NPs. Furthermore, GPU NPs and saline treated blood also observed a decrease in size of the blood clot, indicated by the decrease in absorbance of the blood samples with time (Figure 3C).

The cell uptake of coumarin-6 loaded GPUs was determined by measuring the fluorescence (as an indicator of NPs internalized into cells) normalized to the amount of proteins (as a determinant of cell number) using a spectrophotometer (Figure 4A). Coumarin-6 loaded GPUs observed a NP concentration dependent uptake into A549 lung cancer cells, with significantly higher amounts of NPs up taken at the 250 μg/ml dose compared to lower doses. Fluorescence microscopy also revealed a dose-dependent accumulation of GPUs

(bright green dots) within A549 lung cancer cells and their microenvironment, where higher concentrations of NPs accumulated at a higher number compared to cells treated with lower concentrations of GPUs (Figure 4B).

3.3 *In vitro* lung cancer cell killing

The therapeutic efficacy of CGPUs was determined by exposing A549 lung cancer cells to the cisplatin loaded NPs, and determining the treatment induced cell death via cytotoxicity assays and CFA assays. The significant cisplatin dose-dependent cell death of the A549 lung cancer cells over a 72-hour period were observed when the A549 cells were exposed to the treatment groups (CGPU) compared with free cisplatin of equivalent concentrations. Within 72 hours, CGPUs treatment significantly increased the cancer cell death (~70%), especially at higher drug concentrations (5 μg/ml of cisplatin), compared to those treated with free cisplatin (~ 60%) and CPLGA (~ 30%) (Figure 5A). Notably, there was a significant difference in the cancer killing efficacy even at low drug doses where, CGPU3 and GPU3 (P-value = 0.0001) and that of CGPU3 and CPLGA (P-value = 0.012). The significance difference between GPU3 and CPLGA was 0.29 indicating that the results of these two groups were not significantly different. Figure 3A observed approximately 90% cell viability i.e. ~ 10% cell death within 24 hours of ~ 0.1 mg/mL GPU exposure to the cells, thus the 20% cell death observed in this study after 72 hours at similar NP concentrations used in this study (Figure 5A) could potentially be due to longer NP exposure times. Furthermore, the therapeutic efficacy of the CGPUs were assessed by detecting the amount of caspase-3 produced during the treatment over 72 hours. Caspase-3 production is a marker of cellular apoptosis, indicating cellular death. Similar to the above results tested by LDH assays, the CGPU treatment augmented the caspase-3 production from the A549 cells (~ 86%), compared to free cisplatin (~83%) and CPLGA NPs (~80%) (Figure 5B).

Clonogenic assays were utilized to determine the survival of A549 cancer cell colonies. The A549 cells treated with CGPUs observed a survival fraction of 0.51, which was significantly lower than free cisplatin (0.72), and CPLGA NPs (0.56) (Figure 5C). A similar trend in cancer cell killing was observed via live/dead staining where CGPUs showed a larger number of dead cells (red colored cells) compared to those treated with free cisplatin (Figure 5D). The CGPUs also showed better *in vitro* therapeutic efficacy than the cisplatin loaded PLGA NPs (CPLGA).

3.4 *In vivo* biodistribution study

In vivo biodistribution studies were performed to determine the localization of the GPUs in the tumor and other organs in the animal body. The nude mice bearing subcutaneously implanted A549 lung tumors were injected with cyanine-7 loaded GPUs to determine NP enrichment efficacy with saline as a background control. After 24 hours NP administration, the mice, tumors, and visceral tissues were imaged *ex vivo* and NP localization in the tissues was calculated using Equation 3 (Figure 6A). The mice administered with the GPUs observed 6.5 ± 1.4% (of total injected NPs, %ID/g of tissue) accumulation in the tumor tissues within 24 hours of administration (Figure 6B), which could potentially be due to the enhanced permeability and retention (ERP) effects of tumor blood vessels that improve the chances of the NPs to be retained in the tumor regions. In addition, we observed NP

localization in the liver (29.3 ± 7.8%), kidneys (20.5 ± 4.8%), and spleen (7.4 ± 1.6%). Our observations from the fluorescence images correlated with our analysis of homogenized organs, where higher amounts of GPUs were observed to localize more in the visceral organs than in the tumor.

3.5 *In vivo* tumor growth inhibition

The tumor growth rates (TGR, calculated by Equation 4 and 5) of the mice treated with saline and bare NPs exhibited an increase in relative tumor volume with time (Figure 6C). During the 14-day treatment period, the TGR of mice administered with saline increased from 1 to 13, while those administered with bare GPUs increased from 1 to 12.2, indicating no effect of the bare NPs on the tumor growth. The mice administered with free cisplatin exhibited an increase in relative tumor volume, but the TGR (1 to 5.9) was slower than those for the saline and bare NPs. However, mice treated with CGPUs observed a TGR of 1.5 within 14 days indicating a negligible change in the TGR. These results were further verified using *ex vivo* representative photographs of tumors excised from the various groups that exhibited the differences in tumor sizes across the groups (Figure 6D).

4. DISCUSSION

The GSH/glutathione disulfide (GSSG) is the major redox couple in mammalian cells, and it is a major determinant of the anti-oxidative capacities of cells, while extending cell-protection against free radicals [18]. The intracellular GSH/GSSG levels are regulated by various redox couples, like $NADH/NAD^+$, $NADPH/NADP^+$ and $thioredoxin_{red}/thioredoxin_{ox}$ [18]. GSH dysregulation plays a key role in human cancers, often increasing cellular resistance to several chemotherapeutic drugs [19]. Since tumor tissues express immensely higher levels of GSH (~2–10 mM) compared to normal tissues (~2–10 μM), GSH is a valuable endogenous tool to trigger drug release from polymers exhibiting GSH-responsive behaviors [8, 18].

The most common approach to GSH-responsive materials involves incorporation of disulfide linkages in the polymer backbone that scavenge GSH, undergo reduction and subsequent disassembly to release their payload. For example, amphiphilic copolymers containing disulfide linkages were utilized for drug release in response to elevated GSH levels [20]. However, these micelles observed poor sensitivity to GSH levels up to 10 mM of GSH but demonstrated an increased drug release with 30 mM of GSH. An amphiphilic graft copolymer of hydrophobic poly(amidoamine) and poly(ethylene glycol) incorporating disulfide linkages observed nearly 100% drug release within 10 hours of exposure to 1 mM of DTT [21]. However, over 25% of the drug was released within the same timeframe in the absence of DTT, which is significantly higher compared to our observation (5% within 100 hours in the absence of GSH for CGPU NPs). In another approach, mesoporous silica NPs capped with disulfide linkages on their surface were coated with N-acetylated heparin encapsulating doxorubicin [22]. These NPs showed a GSH concentration sensitive increase in doxorubicin with approximately 100% release within 24 hours upon exposure to 10 mM of GSH and ~20% release in the absence of GSH, which is significantly higher than that observed from our NPs (~5% cisplatin release in the absence of GSH). Our NPs observed

distinctive sensitivity to GSH levels at 5 mM and 10 mM of GSH, with 5-times and 10-times more drug release compared to 0 mM of GSH. These results highlight the sensitivity of our NPs towards GSH levels. The improved GSH sensitivity is potentially due to higher disulfide bonds in the parent polymer, which also increases the hydrophilicity of the polymer [11]. A higher degree of disulfide bonds in the parent polymer could also indicate rapid cleavage of the bonds in reducing the GSH environment, leading to higher drug release rates. Previously, our group also demonstrated that higher disulfide bonds containing polyurethane scaffolds degraded faster *in vitro* and *in vivo* studies [11]. PU-1.8SS (43.6% mass remaining) exhibited the fastest degradation rate compared to PU-0.5SS (87%), PU-1SS (80%), and PU-1.5SS (55%) in 10 mM GSH after 14 days. The presence of GSH cleaved disulfide bonds caused polymer degradation *in vitro*, so the higher disulfide bonds are the quicker degradation. *In vivo* mouse subcutaneous implantation thickness of PU-1.8SS scaffold significantly showed thinner than those of PU-1SS and PU-BDO after 2 months. It indicated that the GSH sensitivity of such polyurethane polymers could be tuned by altering disulfide contents in the polymer backbone, which is very important when such NPs are used for lung cancer treatment.

The CGPUs significantly out-performed cisplatin-loaded PLGA NPs that are conventionally used as drug carriers for chemotherapy due to their biodegradable and biocompatible natures [23]. Moreno et al. [24], observed tumor bearing mice treated with cisplatin-loaded PLGA NPs exhibited a tumor inhibition similar to free cisplatin, while the NPs group showed less toxicity side-effect than free cisplatin. However, our observation of *in vivo* therapeutic efficacies witnessed a plateau in tumor growth rates in the mice treated with CGPUs, while mice treated with free cisplatin observed a significant increase in tumor growth rates at the same drug dose. These results might be due to the stimuli-responsive “on-demand” drug release from the GSH-responsive nanoparticles. Similarly, Ryu et al. [20], observed about 80% viability of MCF-7 breast cancer cells treated with doxorubicin-loaded GSH-responsive micelles. The addition of exogenous GSH further decreased cell viability to 30% for cells treated with 20 mM of GSH in addition to the Dox-loaded micelles. Our results observed that CGPUs significantly reduced the viability of A549 lung cancer cells (up to 70% cell death) compared to free cisplatin (up to 60% cell death) at equivalent concentrations without the addition of GSH. Additionally, our CGPU NPs showed higher sensitivity of GSH concentrations compared to those synthesized by Ryu et al [20], thus contributing to enhanced therapeutic efficacy.

Since the end goal of CGPUs is to augment the cancer killing ability of chemotherapeutic drugs, it is imperative to determine this ability in *in vivo* tumor models. The cancer killing ability and tumor localization of CGPUs were investigated in athymic nude mice implanted with A549 lung cancer cells on their hindlimb. Our major findings indicate significantly higher localization of the NPs in the organs such as liver and kidney, with a comparatively meager 7% GPUs localized in the tumor, an outcome often witnessed by intravenous drug delivery [25]. The fast clearance of the NPs from the kidneys, could be due to clearance of the small sized NPs and small molecular weight dyes [26]. We also speculated that the stimuli responsive release of cyanine 7 dye from the dye-loaded GPUs within the tumor microenvironment might also contribute to the accumulation in the kidney. These results are supported by the observations of Wu et al [25], where 24 hours post injection significant

amount of cyanine 7 was cleared by the kidneys. The remaining NPs, which were not observed to localize in the tumors, liver, kidneys or spleen in our animal studies, may be lost at the injection site during tail vein injection, localized in other organs, including heart, or circulating in plasma as observed in other studies [25, 27–29]. Furthermore, we do not observe a clear correlation between the fluorescence images and the results obtained from homogenized tissues, and it might be due to a result of autofluorescence artifact in the fluorescence images [29]. This effect is possibly eliminated by subtracting the background in homogenized samples. These results noted that although GPUs could be localized in the tumor regions, lack of specificity and targeting would drive their accumulation into other organs. Similar results were observed by He et al [30], where 8.5% of injected untargeted NPs accumulated in the tumors. Furthermore, a comprehensive study looking at the tumor localization efficiency of nanoparticles *via* passive transport in rodents, observed between 0.01 to 28.8% NP localization, indicating that the 7% GPU localization observed in our study contends with commonly observed results [31]. It is also important to consider the heterogeneity of the EPR effect, as result of which the low engraftment may be sufficient to achieve better therapeutic results than the chemotherapeutic drugs [32]. Based on our *in vivo* tumor killing study in a similar tumor model, we also observed that CGPUs with such percentile in the tumor are able to deliver cisplatin and curb tumor growth than that of free cisplatin, thus producing promising therapeutic outcomes.

Limitations of this study include the use of subcutaneous tumor models instead of orthotopic lung tumor models that would provide a more relevant microenvironment to study the therapeutic efficacies and biodistribution of the NPs [33]. The intracellular GSH concentration has been reported variously with different cancer types in literatures. Although the GSH level in lung cancer tissues is significantly higher than other tissues, it is unclear whether the amount of GSH in NSCLC is enough to trigger drug release. Our NPs will release a drug effectively in the presence of GSH concentrations at 5 mM and 10 mM. Rowell et al. [34], reported that the GSH concentration in lung cancer patients was 2.76 mM, while the concentration in a normal lung was 1.04 mM. The GSH level is quite low to trigger a drug release. It was reported that glutathione levels in lung cancers varied 1 to 3 μmol/g-tissue from 10 different studies [35]. Thus, it is hard to know how effectively NPs release drugs in lung cancer patients. However, it is feasible to include more disulfide bonds in the polymer to increase the GSH sensitivity. Furthermore, grafting lung cancer cell targeting moieties on the CGPUs, and use of local drug delivery techniques, such as direct inhalation delivery of the NPs to the lung, may support specific localization and enrichment of the NPs at the tumor site [36], which is our future work.

5. CONCLUSION

We developed glutathione-responsive polyurethane NPs specifically to address the need for effective therapeutics for lung cancer. The particles were stable up to 48 hours in the culture medium and exhibited a glutathione concentration dependent release of cisplatin up to 5 days. They showed good cyto-compatibility to AT1 lung cells, hemocompatibility to human blood, and concentration-dependent uptake into A549 lung cancer cells. Furthermore, the cisplatin-loaded GPUs significantly reduced the tumor growth rate *in vivo* compared to the free cisplatin in a subcutaneously implanted murine A549 lung tumor model. The cisplatin

loaded glutathione-responsive NPs have great opportunities to be further investigated and utilized to enhance chemotherapeutic efficiency for lung cancer treatment.

ACKNOWLEDGEMENTS

We gratefully acknowledge the partial support from the National Heart, Lung and Blood Institute grant (#T32HL134613, KTN) and the National Science Foundation CAREER grant (#1554835, YH).

REFERENCES

[1]. Siegel RL, Miller KD, Jemal A Cancer statistics, 2018. CA Cancer J Clin, 68 (2018), pp. 7–30. [PubMed: 29313949]

[2]. Sukumar UK, Bhushan B, Dubey P, Matai I, Sachdev A, Packirisamy G Emerging applications of nanoparticles for lung cancer diagnosis and therapy. Int Nano Lett, 3 (2013), pp. 45.

[3]. Sarin N, Engel F, Kalayda GV, Mannewitz M, Cinatl J Jr., Rothweiler F, Michaelis M, Saafan H, Ritter CA, Jaehde U, Frotschl R Cisplatin resistance in non-small cell lung cancer cells is associated with an abrogation of cisplatin-induced G2/M cell cycle arrest. PLoS One, 12 (2017), pp. e0181081. [PubMed: 28746345]

[4]. Pignon JP, Tribodet H, Scagliotti GV, Douillard JY, Shepherd FA, Stephens RJ, Dunant A, Torri V, Rosell R, Seymour L, Spiro SG, Rolland E, Fossati R, Aubert D, Ding K, Waller D, Le Chevalier T Lung adjuvant cisplatin evaluation: a pooled analysis by the LACE Collaborative Group. J Clin Oncol, 26 (2008), pp. 3552–3559. [PubMed: 18506026]

[5]. Peng XH, Wang Y, Huang D, Wang Y, Shin HJ, Chen Z, Spewak MB, Mao H, Wang X, Wang Y, Chen ZG, Nie S, Shin DM Targeted delivery of cisplatin to lung cancer using ScFvEGFR-heparin-cisplatin nanoparticles. ACS Nano, 5 (2011), pp. 9480–9493. [PubMed: 22032622]

[6]. Lee W-H, Loo C-Y, Traini D, Young PM Inhalation of nanoparticle-based drug for lung cancer treatment: Advantages and challenges. Asian J Pharm Sci, 10 (2015), pp. 481–489.

[7]. Menon JU, Kuriakose A, Iyer R, Hernandez E, Gandee L, Zhang S, Takahashi M, Zhang Z, Saha D, Nguyen KT Dual-drug containing core-shell nanoparticles for lung cancer therapy. Sci Rep, 7 (2017), pp. 13249. [PubMed: 29038584]

[8]. Mura S, Nicolas J, Couvreur P Stimuli-responsive nanocarriers for drug delivery. Nat Mater, 12 (2013), pp. 991–1003. [PubMed: 24150417]

[9]. Zhou L, Wang H, Li Y Stimuli-responsive nanomedicines for overcoming cancer multidrug resistance. Theranostics, 8 (2018), pp. 1059–1074. [PubMed: 29463999]

[10]. Traverso N, Ricciarelli R, Nitti M, Marengo B, Furfaro AL, Pronzato MA, Marinari UM, Domenicotti C Role of glutathione in cancer progression and chemoresistance. Oxidative Med Cell Longev, 2013 (2013), pp. 10.

[11]. Xu C, Huang Y, Wu J, Tang L, Hong Y Triggerable degradation of polyurethanes for tissue engineering applications. ACS Appl Mater Interfaces, 7 (2015), pp. 20377–20388. [PubMed: 26312436]

[12]. Iyer R, Kuriakose AE, Yaman S, Su LC, Shan D, Yang J, Liao J, Tang L, Banerjee S, Xu H, Nguyen KT Nanoparticle eluting-angioplasty balloons to treat cardiovascular diseases. Int J Pharm, 554 (2019), pp. 212–223. [PubMed: 30408532]

[13]. Basotra M, Singh SK, Gulati M Development and validation of a simple and sensitive spectrometric method for estimation of cisplatin hydrochloride in tablet dosage forms: application to dissolution studies. ISRN Anal Chem, 2013 (2013), pp. 8.

[14]. Xu H, Nguyen KT, Brilakis ES, Yang J, Fuh E, Banerjee S Enhanced endothelialization of a new stent polymer through surface enhancement and incorporation of growth factor-delivering microparticles. J Cardiovasc Transl Res, 5 (2012), pp. 519–527. [PubMed: 22639344]

[15]. Franken NA, Rodermond HM, Stap J, Haveman J, van Bree C Clonogenic assay of cells in vitro. Nat Protoc, 1 (2006), pp. 2315–2319. [PubMed: 17406473]

[16]. Kim JC, Saha D, Cao Q, Choy H Enhancement of radiation effects by combined docetaxel and flavopiridol treatment in lung cancer cells. Radiother Oncol, 71 (2004), pp. 213–221. [PubMed: 15110456]

[17]. Prinsen K, Li J, Vanbilloen H, Vermaelen P, Devos E, Mortelmans L, Bormans G, Ni Y, Verbruggen A Development and evaluation of a 68Ga labeled pamoic acid derivative for in vivo visualization of necrosis using positron emission tomography. Bioorg Med Chem, 18 (2010), pp. 5274–5281. [PubMed: 20580560]

[18]. Cheng R, Feng F, Meng F, Deng C, Feijen J, Zhong Z Glutathione-responsive nano-vehicles as a promising platform for targeted intracellular drug and gene delivery. J Control Release, 152 (2011), pp. 2–12. [PubMed: 21295087]

[19]. Ortega AL, Mena S, Estrela JM Glutathione in cancer cell death. Cancers, 3 (2011), pp. 1285–1310. [PubMed: 24212662]

[20]. Ryu JH, Roy R, Ventura J, Thayumanavan S Redox-sensitive disassembly of amphiphilic copolymer based micelles. Langmuir, 26 (2010), pp. 7086–7092. [PubMed: 20073533]

[21]. Sun Y, Yan X, Yuan T, Liang J, Fan Y, Gu Z, Zhang X Disassemblable micelles based on reduction-degradable amphiphilic graft copolymers for intracellular delivery of doxorubicin. Biomaterials, 31 (2010), pp. 7124–7131. [PubMed: 20580429]

[22]. Dai L, Li J, Zhang B, Liu J, Luo Z, Cai K Redox-responsive nanocarrier based on heparin end-capped mesoporous silica nanoparticles for targeted tumor therapy in vitro and in vivo. Langmuir, 30 (2014), pp. 7867–7877. [PubMed: 24933090]

[23]. Acharya S, Sahoo SK PLGA nanoparticles containing various anticancer agents and tumour delivery by EPR effect. Adv Drug Deliv Rev, 63 (2011), pp. 170–183. [PubMed: 20965219]

[24]. Moreno D, Zalba S, Navarro I, Tros de Ilarduya C, Garrido MJ Pharmacodynamics of cisplatin-loaded PLGA nanoparticles administered to tumor-bearing mice. Eur J Pharm Biopharm, 74 (2010), pp. 265–274. [PubMed: 19883755]

[25]. Wu Y, Cai W, Chen X Near-infrared fluorescence imaging of tumor integrin alpha v beta 3 expression with Cy7-labeled RGD multimers. Mol Imaging Biol, 8 (2006), pp. 226–236. [PubMed: 16791749]

[26]. Longmire M, Choyke PL, Kobayashi H Clearance properties of nano-sized particles and molecules as imaging agents: considerations and caveats. Nanomedicine, 3 (2008), pp. 703–717. [PubMed: 18817471]

[27]. Ling X, Tu J, Wang J, Shajii A, Kong N, Feng C, Zhang Y, Yu M, Xie T, Bharwani Z, Aljaeid BM, Shi B, Tao W, Farokhzad OC Glutathione-responsive prodrug nanoparticles for effective drug delivery and cancer therapy. ACS Nano, 13 (2019), pp. 357–370. [PubMed: 30485068]

[28]. Sykes EA, Dai Q, Tsoi KM, Hwang DM, Chan WCW Nanoparticle exposure in animals can be visualized in the skin and analysed via skin biopsy. Nat Commun, 5 (2014), pp. 3796. [PubMed: 24823347]

[29]. Jun YW, Kim HR, Reo YJ, Dai M, Ahn KH Addressing the autofluorescence issue in deep tissue imaging by two-photon microscopy: the significance of far-red emitting dyes. Chem Sci, 8 (2017), pp. 7696–7704. [PubMed: 29568432]

[30]. He H, Guo C, Wang J, Korzun WJ, Wang XY, Ghosh S Leutusome: A biomimetic nanoplatform integrating plasma membrane components of leukocytes and tumor cells for remarkably enhanced solid tumor homing. Nano Lett, 18 (2018), pp. 6164–6174. [PubMed: 30207473]

[31]. Björnmalm M, Thurecht KJ, Michael M, Scott AM, Caruso F Bridging bio–nano science and cancer nanomedicine. ACS Nano, 11 (2017), pp. 9594–9613. [PubMed: 28926225]

[32]. Golombek SK, May JN, Theek B, Appold L, Drude N, Kiessling F, Lammers T Tumor targeting via EPR: Strategies to enhance patient responses. Adv Drug Deliv Rev, 130 (2018), pp. 17–38. [PubMed: 30009886]

[33]. Killion JJ, Radinsky R, Fidler IJ Orthotopic models are necessary to predict therapy of transplantable tumors in mice. Cancer Metastasis Rev, 17 (1998), pp. 279–284. [PubMed: 10352881]

[34]. Rowell NP, McCready VR, Cronin B, Pepper J, Higley B, Burke JF, Tyrrell DA 99Tcm-labelled meso-HMPAO and glutathione content of human lung tumours. Nucl Med Commun, 10 (1989), pp. 503–508. [PubMed: 2552364]

[35]. Gamcsik MP, Kasibhatla MS, Teeter SD, Colvin OM Glutathione levels in human tumors. Biomarkers, 17 (2012), pp. 671–691. [PubMed: 22900535]

[36]. Azarmi S, Roa WH, Lobenberg R Targeted delivery of nanoparticles for the treatment of lung diseases. Adv Drug Deliv Rev, 60 (2008), pp. 863–875. [PubMed: 18308418]

Highlights:

- Glutathione is abundantly available in lung cancer microenvironment.
- Biodegradable polyurethane nanoparticles were fabricated via a single emulsion with a mixed organic solvent.
- GSH-sensitive biodegradable polyurethane nanoparticles (GPUs) released encapsulated cisplatin in response to elevated glutathione levels.
- Cisplatin loaded GPUs significantly reduced tumor growth in a subcutaneously xenograft A549 lung tumor mouse model compared to the free cisplatin.

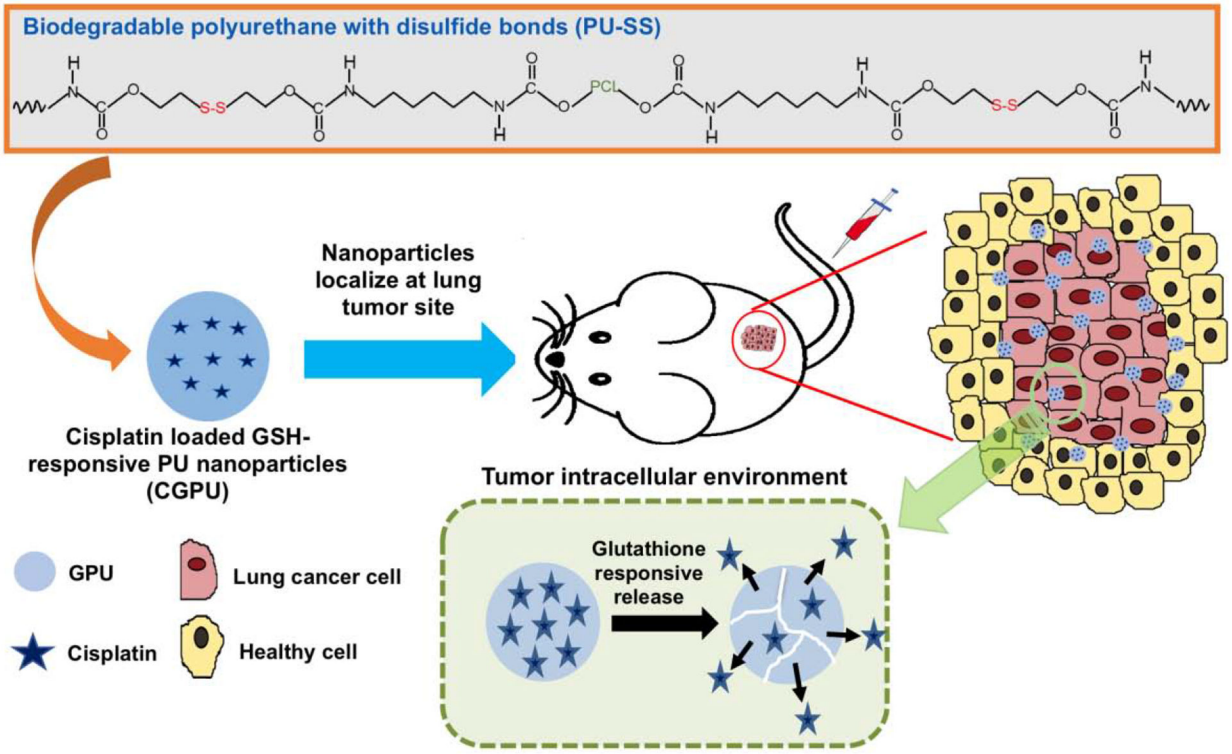

Figure 1.

Illustration to develop GSH responsive polyurethane nanoparticles loaded with an anticancer drug for lung cancer treatment. The polyurethane with disulfide bonds (PU-SS) was fabricated into the nanoparticles loaded with model anticancer drug cisplatin (CGPU). The CGPU NPs were injected into a lung cancer bearing mouse model through tail IV, and the NPs released cisplatin at a high GSH level environment inside the tumor to kill the lung cancer cells.

A)

	Nanoparticle size (nm)	Zeta potential (mV)
GPU	189 ± 21	-14±4
CGPU	245 ± 20	-12± 2

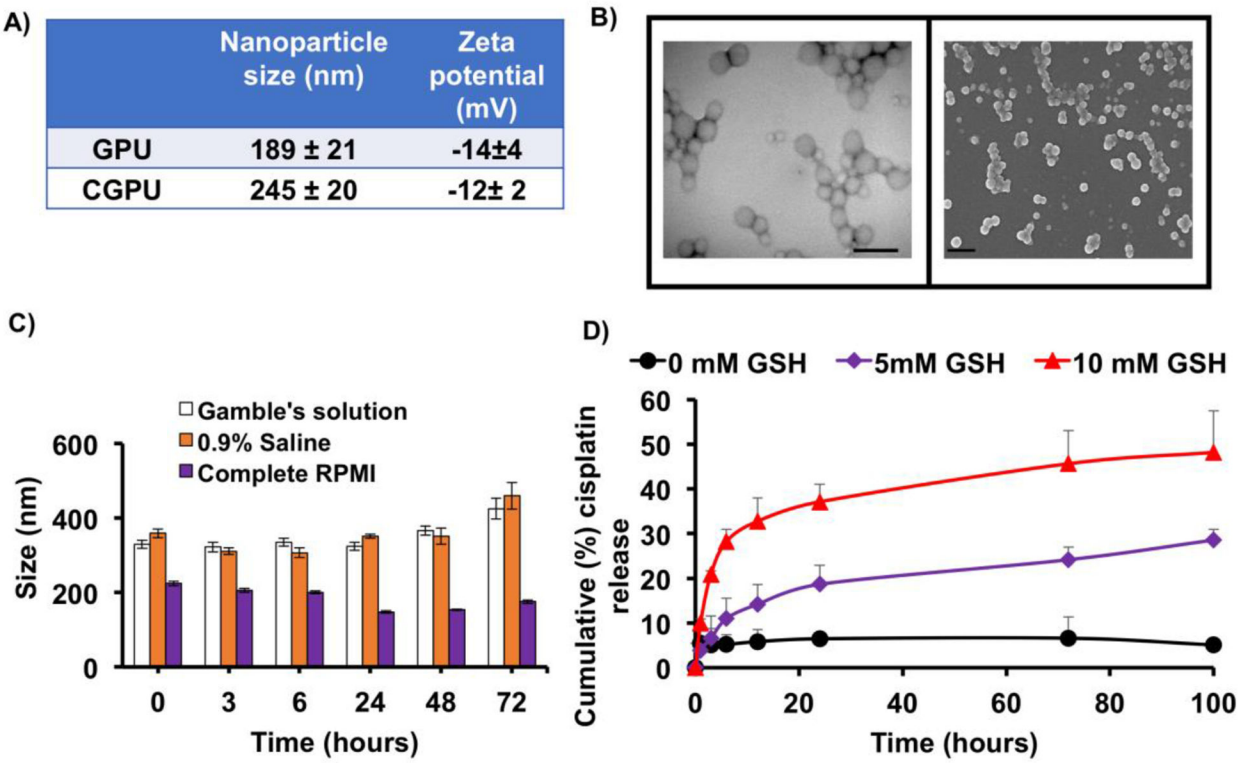

Figure 2.

Nanoparticle characterization. A) Size and zeta potential of GSH sensitive NPs via dynamic light scattering (DLS). B) TEM (left; scale bar: 500nm) and SEM (right; scale bar: 500nm) images of GSH sensitive NPs observe smooth morphology. C) NP stability evaluated by changes in the NP size over time in gamble's solution (stimulated lung fluid), 0.9% saline, and complete cell culture media (RPMI) up to 48 hours. D) CGPUs exposed to 5 mM and 10 mM of GSH experienced significantly higher drug release, compared to 0mM of GSH.

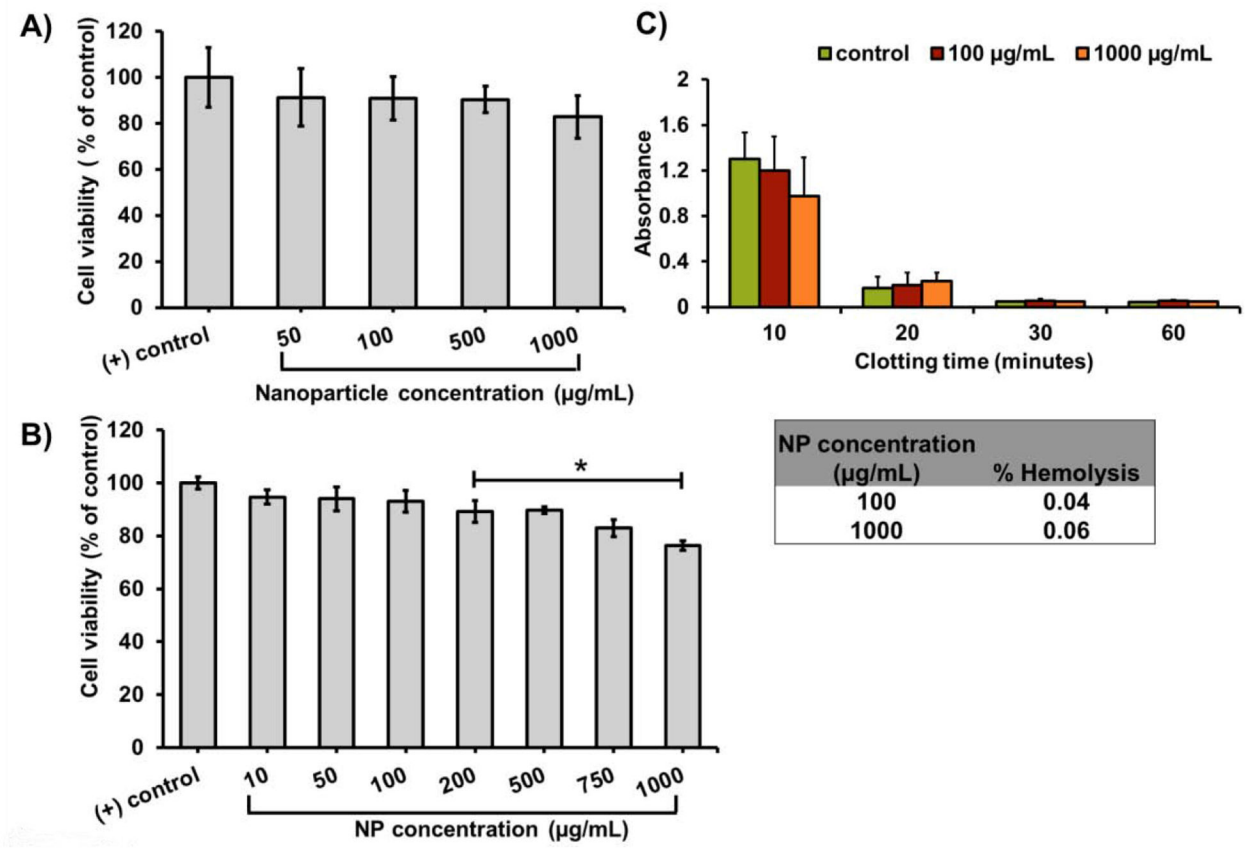

Figure 3.

In vitro cytocompatibility and blood compatibility of GPUs. A) *In vitro* cyto-compatibility studies of GPUs observed over 80% viability of alveolar type-I cells via MTS assays. B) LIVE/DEAD cell viability assays also observed AT1 survival over 90% of AT1 survival at the highest NP concentration (* $p < 0.05$ vs. (+) control/complete media). C) GPUs observed low hemolysis (inset), and a blood clotting trend similar to that of saline control confirmed by the blood clotting profile.

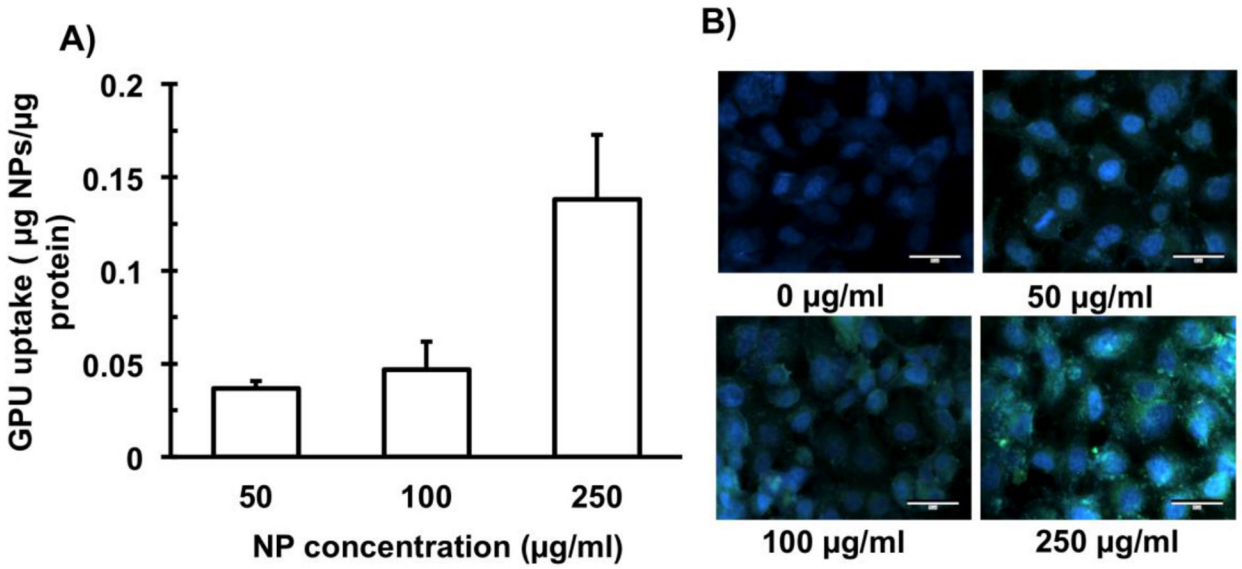

Figure 4.

In vitro cell uptake study of GPUs. **A)** Fluorescently labeled GPUs observed dose-dependent NP cellular uptake to A549 cells. **B)** Representative fluorescence microscopy images observed NP concentration-dependent localization of GPUs (bright green dots) in the lung cancer cells. Scale bar: 30 µm.

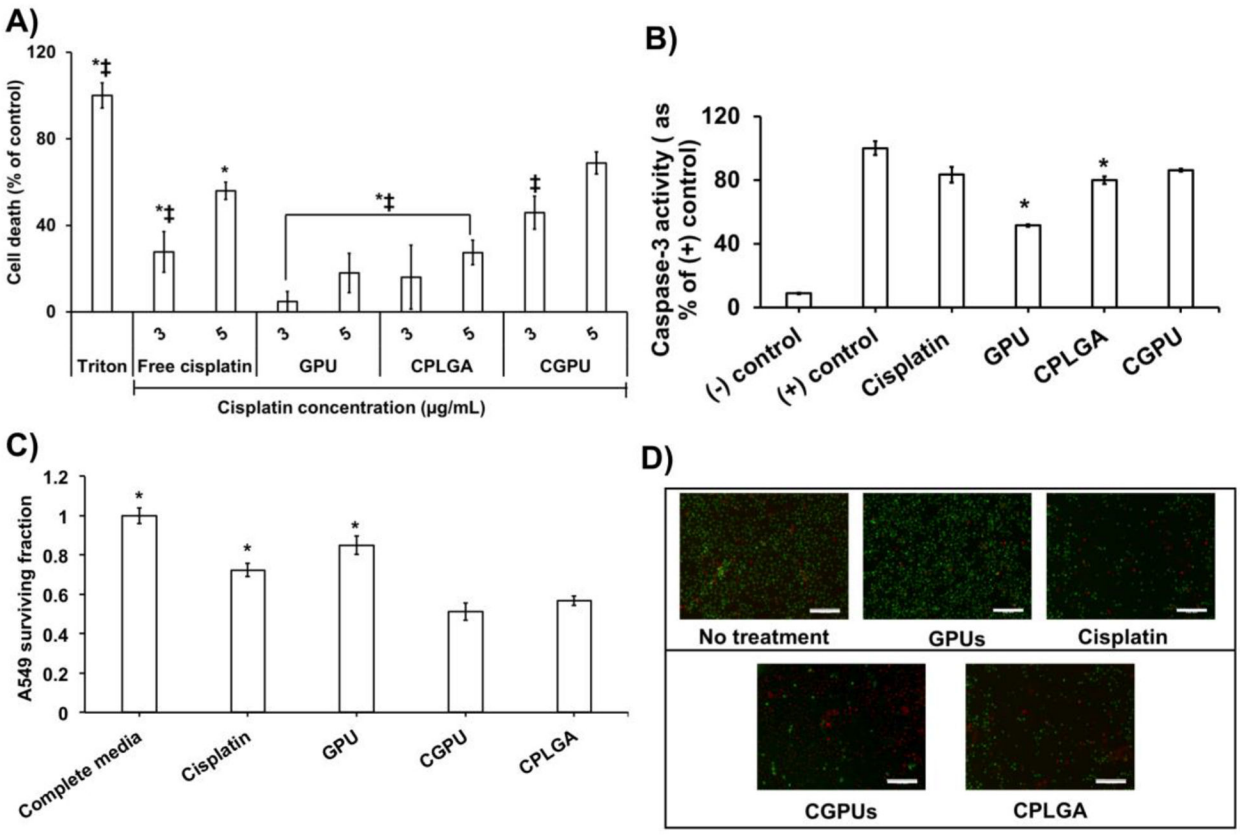

Figure 5.

In vitro lung cancer cell killing assessment of CGPUs. CGPU showed significant improvement in A549 lung cancer cell survival via: A) LDH assays depicting higher cell death of A549 cells treated with CGPUs (* $P<0.05$ vs. CGPU NPs equivalent to 3 μg/mL of cisplatin and ‡ $P<0.05$ vs. CGPU NPs equivalent to 5 μg/mL of cisplatin). GPU concentrations of 60 μg/mL and 100 μg/mL corresponding to 3 μg/mL and 5 μg/mL cisplatin groups, respectively, were used for this study. B) Caspase-3 assays observed significantly higher caspase-3 production by A549 cells treated with CGPUs (* $P<0.05$ vs. CGPU). C) Reduced survival fraction of A549 cells treated with CGPU compared to that of free cisplatin by colony formation assays (* $P<0.05$ vs. CGPU). D) A549 cells treated with CGPUs showed higher density of dead cells (red) compared to live cells (green) by live/dead fluorescence imaging (scale bar: 100 μm).

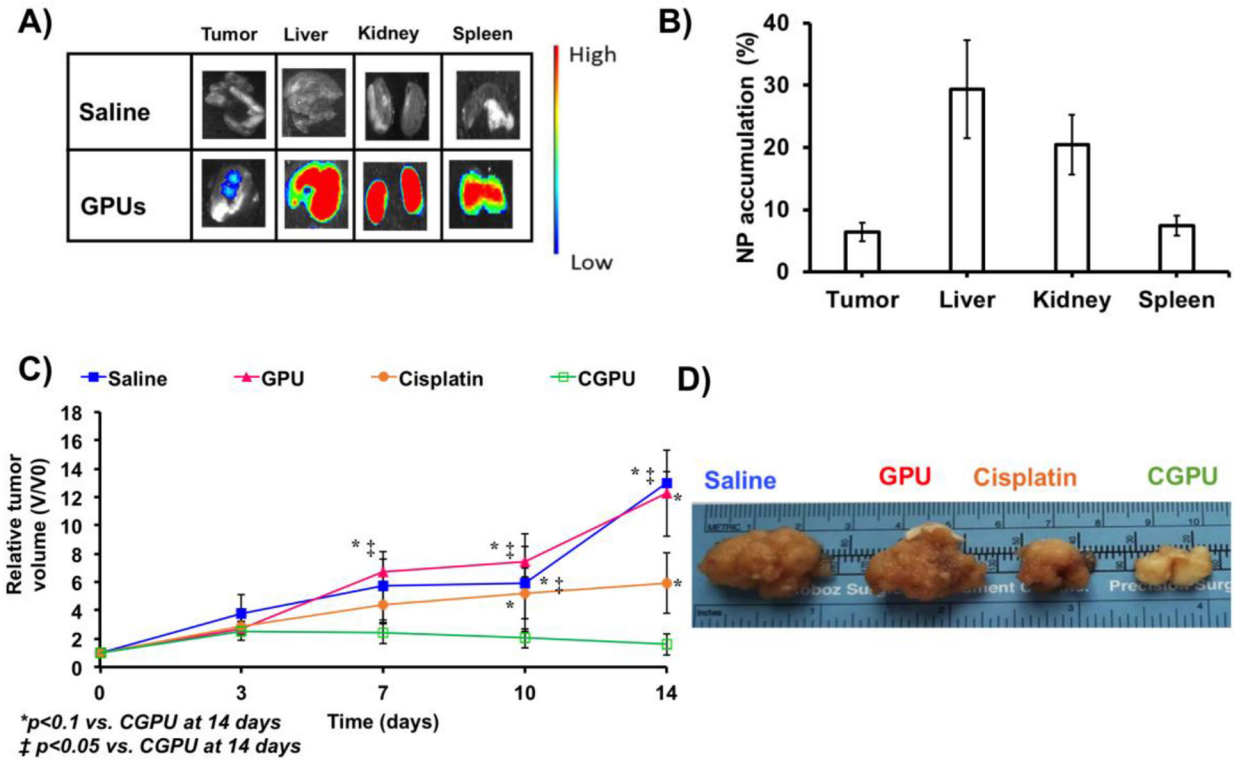

Figure 6.

In vivo distribution and therapeutic efficacy study. A) *In vivo* fluorescence imaging observed cyanine 7 loaded GPU localization in tumor tissues within 24 hours of administration to mice bearing subcutaneously implanted lung tumors. B) *Ex vivo* analysis of tumor homogenates observed ~7% accumulation of GPUs in the lung tumor site. C) A549 tumor growth rate significantly declined and slowed down in mice treated with CGPUs, compared to those by the free cisplatin, GPUs and saline (control). *P < 0.05 vs. CGPUs_14 days and ‡P< 0.1 vs. CGPUs_14 days. D) *Ex vivo* photographical representation of excised tumors observed smaller tumor sizes in the mice administered with CGPUs.